CrossMark

ORIGINAL ARTICLE

Thermal evolution of aliphatic and aromatic moieties of asphaltenes from coals of different rank: possible implication to the molecular architecture of asphaltenes

Aminu Bayawa Muhammad[1]

Abstract The compositional and structural changes that coal asphaltenes undergo with increasing thermal maturation were investigated using solid-state ^{13}C NMR and Fourier transform infrared spectroscopy. The results show a gradual increase in the relative proportion of carbon content with a concomitant decrease in the hydrogen, sulphur and oxygen content. The amount of aromatic carbon also increases while the aliphatic carbon decreases with increasing maturity. Ester and carboxylic groups are particularly sensitive to maturation and decrease in relative abundance with increasing maturity while the amount of aromatic carbonyl groups increases. In general, the asphaltenes were observed to evolve towards a more thermally stable structure with increasing amounts of aromatic moieties and relatively lower amounts of aliphatic moieties. The results are in agreement with the ultimate dominance of the island molecular architecture (the Yen–Mullins model) in asphaltenes.

Keywords Asphaltenes · Coals · FTIR · Solid-state ^{13}C NMR · Thermal maturation

1 Background

Asphaltenes are complex mixture of carbonaceous macromolecular substances that have been associated with many problems including obstruction of reservoirs, plugging of wells and pipelines as well as fouling and stabilisation of oil–water emulsions in the petroleum industry (Galoppini 1994; Kokal and Sayegh 1995; Khadim and Sarbar 1999; Shedid and Zekri 2006; Ma et al. 2008). Although the term is mainly applied to the heaviest components of petroleum, its functional solubility-based definition allows extension to include similar substances from coals and bitumens (Behar et al. 1984; William 1985; Solli and Leplat 1986) and compositionally the two are quite similar (Badre et al. 2006).

The composition of asphaltenes has been a subject of many investigations (Bunger and Li 1981; Peters 1986; Sheu and Mullins 1995; Sheu 2002; Sabbah et al. 2011; Mullins et al. 2012; Muhammad and Abbott 2013; Wu et al. 2013). In general asphaltenes macromolecules are considered to consist of aliphatic side-chains linked to aromatic moieties via C–C, C–O and C–S bonds (Yen 1974; Peng et al. 1997). The aromatic moieties consist largely of condensed pericyclic sheets of 4 and 20 rings (Groenzin and Mullins 1999; Badre et al. 2006) while the alkyl moieties have been shown to average at C_3 to C_7 in size (Calemma et al. 1995), although homologues in range of C_1 to over C_{32} have observed (del Rio et al. 1995; Peng et al. 1999; Muhammad and Abbott 2013). Furthermore, the aliphatic moieties have been found to consists of both acyclic (*n*-alkyl and *iso*-alkyl) and cyclic (hopanoids, steroids etc.) alkyl groups (Mojelsky et al. 1992; Trifilieff et al. 1992; Peng et al. 1999; Strausz et al. 1999; Muhammad and Abbott 2013). A more complex structure in which the aromatic moieties in the asphaltenes are further interconnected by aliphatic bridges (i.e. the so called polymeric structure) has been subject of intense debate (Bunger and Li 1981; Hammami et al. 1995; Speight 2004; Badre et al. 2006; Strausz et al. 2008; Mullins 2009).

The effect of thermal stress on the molecular composition of aliphatic moieties and stereochemistry of the alicyclic moieties has been reported (Muhammad and Abbott

✉ Aminu Bayawa Muhammad
ambayawa@yahoo.co.uk

[1] Civil Engineering & Geosciences, Newcastle University, Newcastle upon Tyne, NE1 7RU, UK

Chin. J. Geochem. (2015) 34(3):422–430

423

2013). However, the destructive effect of ruthenium oxide oxidation on aromatic moieties prohibits obtaining a complete picture of the thermal evolution of the asphaltenes. In this paper, NMR and FTIR were employed to reveal the changes undergone by the aromatic moieties, as well as aliphatic moieties, of the asphaltenes with possible consequence on the molecular architecture of these enigmatic complex substances.

2 Materials and methods

2.1 Samples

Four pulverised coal samples, namely North Sea Brent coals C04, C56, C69 [with vitrinite reflectance (R_0) values of 0.40 %, 0.56 %, 0.69 %, respectively] and C15 (R_0 value of 1.50 %) from Harvey Beaumont seam, County Durham, United Kingdom, were used in this investigation. The samples cover the thermal maturation range from late diagenesis ($R_0 = 0.2 \% - 0.450 \%$) through catagenesis ($R_0 = 0.6 \% - 0.9 \%$) into metagenesis ($R_0 = 0.9 \% - 2.0 \%$) stages of transformation of sedimentary organic matter.

2.2 Extraction of bitumen

Known weights of the coal samples were extracted for 72 h with DCM/MeOH mixture (93:7, v/v) using Soxhlet extraction method. The solvent was removed from the extracts by rotary evaporation (30 °C, 25 mmHg) followed by drying under nitrogen stream until a constant weight was obtained.

2.3 Precipitation of asphaltenes and elemental analysis

The coal bitumen, dissolved in 1 cm^3 of DCM, was treated with 40 cm^3 of n-hexane. The mixture was stirred for 2 h and allowed to equilibrate for 24 h. The asphaltenes were recovered by centrifugation (3500 rpm, 15 min) and redissolved in 1 cm^3 DCM followed by re-precipitation with 40 cm^3 of n-hexane. After stirring for 30 min, the asphaltenes were recovered. This was repeated two more times. The dry asphaltenes were extracted with n-hexane for 10 days using the Soxhlet method to remove co-precipitated maltene (Alboudwarej et al. 2002). After drying, carbon, hydrogen, nitrogen and sulphur composition of the asphaltenes were determined using a Carlo Erba 1108 Elemental Analyser. The oxygen content was obtained by difference.

2.4 FTIR measurements and curve-fitting of the spectra

About 1 % (w/w) mixture of the asphaltenes in KBr powder (99.5 % IR spectroscopic grade, Sigma-Aldrich) was prepared with an agate mortar and pestle. 13 mm pellets were prepared from about 200 mg of the homogenised sample/KBr powder using a Specac 15 Ton Manual Hydraulic Press.

Thermo Nicolet Nexus 870 FTIR spectrometer (Thermo Nicolet Corp.), with DTGS KBR detector and XT-KBr beam splitter, was used to acquire the IR spectra in the mid-infrared region (400–4000 cm^{-1}) by co-adding 70 scans at a resolution of 4 cm^{-1}.

Prior to curve-fitting with GRAMS/AI (Thermo Scientific, Inc.), each spectrum was: (i) normalised to the concentration of the asphaltene in the pellets, (ii) baseline corrected using multipoint option, and (iii) smoothened using Savitzky-Golay algorithm to reduce noise. Curve-fitting of relevant spectral regions and assignment of bands were done as described in the literature (Maddams 1980; Painter et al. 1981; Yen et al. 1984; Ibarra et al. 1996). Model trend with best fit (from R^2 values) was adopted in plots of areas of absorption bands against vitrinite reflectance.

2.5 Solid-state ^{13}C NMR measurements

The Soxhlet extracted asphaltene samples were used without further preparation. The solid-state ^{13}C NMR spectra were obtained on a Varian VNMRS 400 spectrometer using a double-resonance (H–X) MAS probe equipped with a 4 mm rotor. All the spectra were obtained at 100.56 MHz with 700 scans. The rotor was spun at 12 kHz. A pulse repetition delay of 2 s and a cross polarization (CP) contact time of 0.50 ms were applied for all the experiments. Modulated (TPPM) decoupling was carried out at a nutation frequency of 76 kHz. Dipolar dephasing (DP) delay was set at 40.0 μs. Spectral referencing is with respect to external neat tetramethylsilane.

The data obtained was used to estimate (Eqs. 1–5): the fractions of the aromatic carbon that is protonated (i.e. tertiary aromatic carbon, $f_a^{a,H}$) and nonprotonated (quaternary aromatic carbon, $f_a^{a,N}$); fraction of the total carbon that is protonated (f_a^H) and nonprotonated (f_a^N); as well as the fraction of the total hydrogen present in the aromatic systems (H_a) (Wilson et al. 1984; Wilson and Vassallo 1985).

$$f_a = \frac{A}{T} = \frac{N + P}{T} = \frac{1.21n + P}{T} = \frac{(1.21)(0.88)M + P}{T}$$

(1)

$$f_a^{aH} = \frac{P}{T} \qquad (2)$$

$$f_a^{a,N} = 1 - f_a^{a,H} \qquad (3)$$

$$f_a^{H} = f_a^{a,H} * f_a \qquad (4)$$

$$H_a = (C/H) * f_a^{a,H} * f_a \qquad (5)$$

3 Results and discussion

3.1 Elemental composition

The percentage carbon content of the asphaltenes increases with increasing maturity of the coals of the coals (Fig. 1a), while atomic O/C and S/C ratios decrease with increase in maturity (Fig. 1). These are similar to observations of Rouxhet et al. (1980) in coals and kerogens. Unlike other elements, however, the relative nitrogen content (N/C ratio) increases with increasing maturity of the coals (Fig. 1d). This might be due to two dynamic processes occurring during the diagenesis of the organic matter. Firstly, relative to carbon, the loss of oxygen and sulphur might occur more rapidly (Fig. 1b, c) than nitrogen (Fig. 1d) as suggested by the stiffness of the gradients of the respective plots of the element against maturity

(Fig. 1). Secondly, a significant proportion of the total nitrogen might be fixed in or transformed into functionalities (e.g. aromatic pyridinic and pyrrolic nitrogen (Baxby et al. 1994)) that are relatively more stable than sulphur and oxygen functional groups. Therefore, although the absolute amounts of the nitrogen might be decreasing with increasing maturity, the overall observable effect is its relative enrichment in the residual organic matter with increasing maturity (Fig. 1d). In general, however all the trends (Fig. 1) appear to stabilise as higher maturity level is approached suggesting the transformation proceeds towards a more stable carbon-rich equilibrium structure.

3.2 Distribution and evolution of carbon in asphaltenes

The solid-state ^{13}C NMR spectra of the asphaltenes revealed two broad peaks between 0–60 and 100–150 ppm (Fig. 2a) which are generally assigned to aliphatic and aromatic carbons, respectively (Weinberg et al. 1983; Wilson and Vassallo 1985) although they can be deconvolved into many peaks assignable to different types of aromatic and aliphatic carbons, respectively (Dutta Majumdar et al. 2013). The values of the aromaticity factor (f_a) obtained (Table 1) are similar to reported carbon
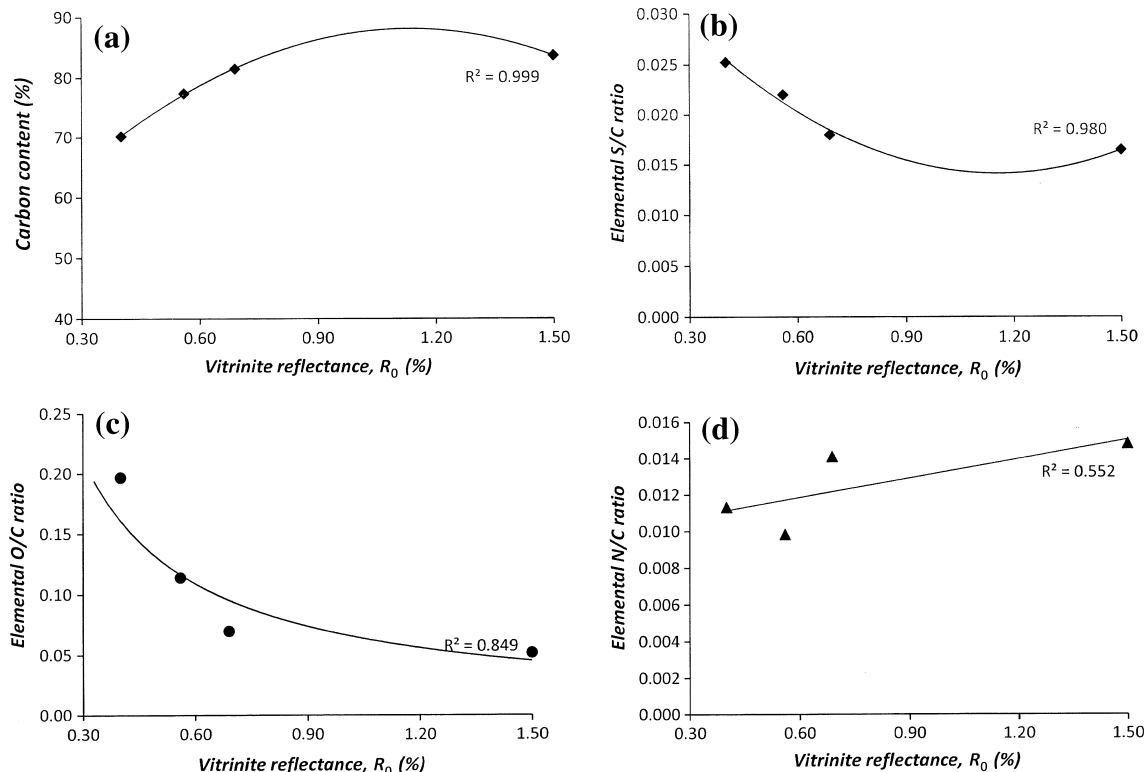

Fig. 1 Plots of (a) %C, (b) O/C, (c) S/C, and (d) N/C against vitrinite reflectance showing the evolution of the relative amounts of elements in the asphaltenes with increasing maturity
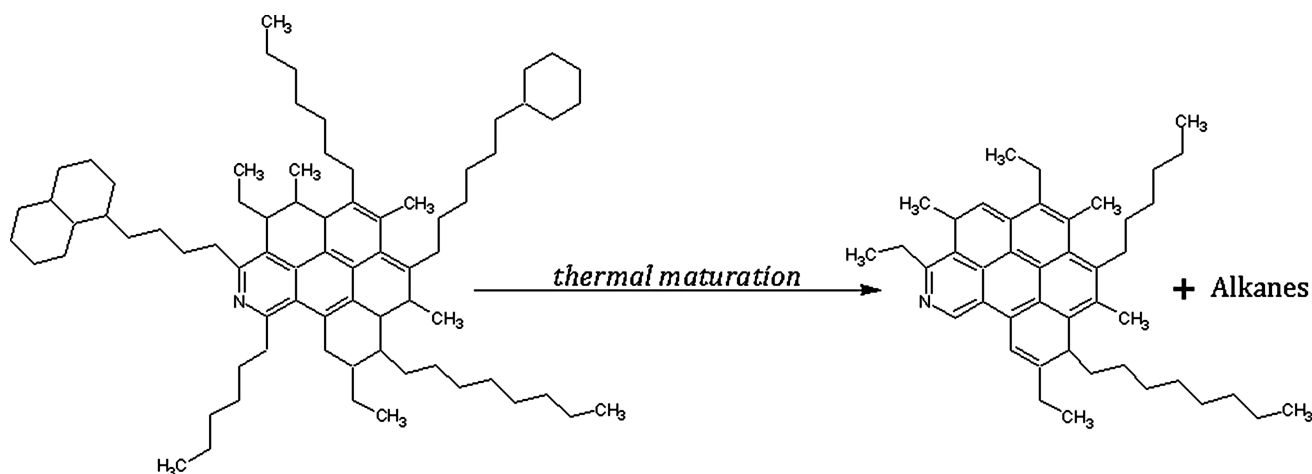
Fig. 2 Molecular illustration showing evolution of aromatic and aliphatic moieties of asphaltene macromolecule with increase in thermal stress

Table 1 Structural parameters calculated from the asphaltenes' solid-state ^{13}C NMR spectra

Sample	C04	C56	C69	C15
Vitrinite reflectance, R_0	0.40	0.56	0.69	1.50
Aromaticity factor, f_a	0.42	0.48	0.56	0.63
Fraction of protonated aromatic carbon, $f_a^{a,H}$	0.34	0.46	0.47	0.43
Fraction of non-protonated aromatic carbon, $f_a^{a,N}$	0.66	0.54	0.53	0.57
Fraction of aromatic carbon, f_a^H	0.14	0.22	0.26	0.27
Fraction of aromatic hydrogen, H_a	0.17	0.28	0.28	0.41

aromaticity of petroleum asphaltenes (Andrews et al. 2011; Dutta Majumdar et al. 2013) although much lower than those of coal asphaltenes (Andrews et al. 2011) possibly due to the effect of thermal liquefaction of the coals (see Sect. 3.4). In general, the aromaticity factor increases with increasing maturity (Table 1) suggesting aromatisation of aliphatic (naphthenic) structures with increasing maturity although dealkylation may also occur simultaneously (Rouxhet et al. 1980; Buch et al. 2003). However, the former is further supported by increase in both the fraction of aromatic hydrogen (H_a) and the fraction of the total carbon that is protonated (tertiary) aromatic carbon (f_a^H) with maturity (Table 1).

Furthermore, the distribution of the aromatic carbon shows that over 50 % of the carbon is in the form of non-protonated (i.e. quaternary) carbon as reflected by $f_a^{a,N}$ although it appears to be independent of maturity (Table 1). It should however be noted that the relatively high value of $f_a^{a,N}$ of C04 asphaltene does not necessarily mean it has more condensed aromatic moieties than the more matured asphaltenes; rather, it may be a reflection of positive contributions to $f_a^{a,N}$ from alkylated (therefore non-protonated) carbons which are more abundant in less mature samples. Thus, as the alkyl groups are replaced with hydrogens following dealkylation with increasing maturity, the apparent proportion of the quaternary carbon ($f_a^{a,N}$) falls

and aromatic hydrogen (H_a) rises (Table 1). In general, increase in the aromaticity of the asphaltene with increasing maturity is mainly due to aromatisation of aliphatic carbon and possibly increasing condensation of the aromatic structures. These observations are consistent with results obtained by Wilson and Vassallo (1985) in their study of distributions of carbon in coals with increasing thermal stress.

3.3 Thermal evolution of functional groups in the asphaltenes

The absorption bands obtained from curve-fitting of the asphaltenes IR spectra are assigned to various functional groups as outlined in Table 2. The O–H/N–H band of the asphaltenes is prominent irrespective of the maturity of the coals suggesting the functionalities are not significantly affected by increase in maturity until at much higher maturation levels (Rouxhet et al. 1980) not covered in this study.

The total absorption due to the five aliphatic C–H stretching vibrations (3000–2800 cm^{-1}) indicative of aliphatic moieties decreases with increase in maturity (Fig. 3a). Furthermore, the intensities of the two alkyl bands at 1455 and 1346 cm^{-1} decrease with increasing maturity (Fig. 3b) indicating dealkylation as the asphaltenes are

Table 2 List and assignment of infrared absorption bands obtained from the curve-fitting of the FTIR spectra of the asphaltenes from the coal samples

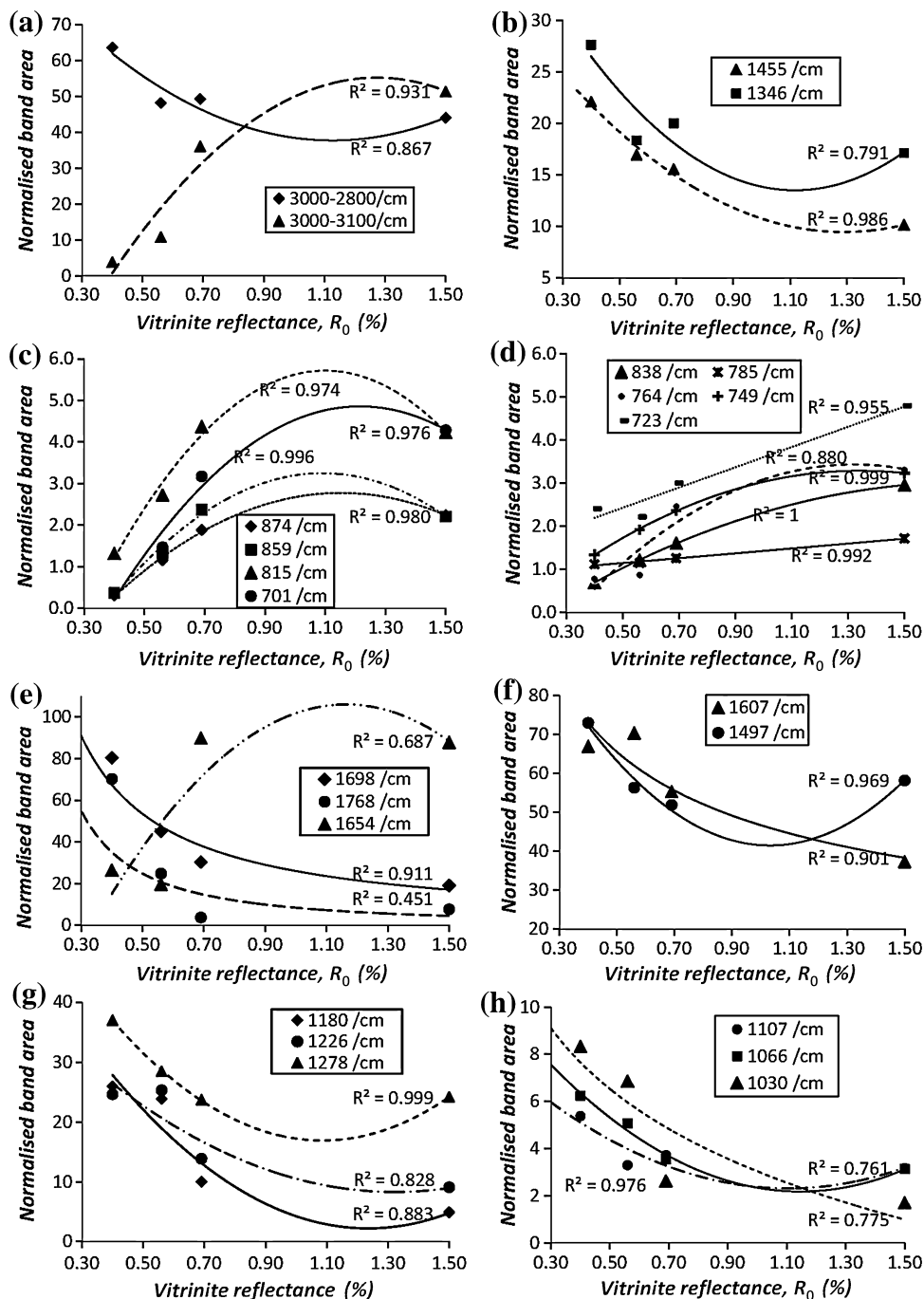| Peak	Peak Centre (cm^{-1})	Assignment
1	3400	ν OH/HN
2	3050	ν C–H aromatic $_ν$
3	3017	ν C–H aromatic
4	2954	as. ν RCH$_3$ aliphatic
5	2923	as. ν R$_2$CH$_2$ aliphatic
6	2897	ν R$_3$CH aliphatic
7	2869	sy. RCH$_3$ aliphatic
8	2851	sy. R$_2$CH$_2$ aliphatic
9	1768	C=O esters
10	1698	C=O carboxyl group
11	1654	C=O conjugated ketone
12	1607	ν C=C aromatic
13	1497	C=C aromatic
14	1455	δ as. CH$_3$−, CH$_2$−
15	1346	δ sy. CH$_2$−C=O
16	1270	ν C–O in aryl ethers
17	1226	ν C–O, δOH, phenoxy & ethers
18	1180	ν C–O phenols & ethers
19	1107	ν C–O tert. Alcohols & ethers
20	1066	ν C–O sec. alcohols
21	1030	ν C–O ethers
22	874	δ 1H—isolated hydrogen on aromatic ring
23	859	δ 1H—isolated hydrogen on aromatic ring
24	838	δ 2H—adjacent hydrogens on aromatic ring
25	815	δ 2H—adjacent hydrogens on aromatic ring
26	785	δ 3H—adjacent hydrogens on aromatic ring
27	764	δ 4H—adjacent hydrogens on aromatic ring
28	749	δ 4H—adjacent hydrogens on aromatic ring
29	723	δ 2H—adjacent hydrogens on aromatic ring
30	701	δ 5H—adjacent hydrogens on aromatic ring

as asymmetric, *sy* symmetric

exposed to increasing thermal stress. All these are in agreement with decrease in aliphatic carbon with increasing maturity as observed from ^{13}C NMR results (Sect. 3.2). This is a further indication that both dealkylation and aromatisation of aliphatic units occur simultaneously as maturity increases as illustrated in Fig. 2. However, the two other bands at 1424 and 1375 cm^{-1}, also commonly assigned to aliphatic moieties appear to be independent of maturity of the coals within the maturity region under investigation.

The aromatic C–H stretching vibrations (3000–3100 cm^{-1}) are barely detectable in the immature C04 asphaltenes but increase with increasing maturity with the strongest absorption observed in C15 asphaltene (Fig. 3a). The evolution of the aromatic structures is further revealed by increase in the intensities of the nine bands between 900 and 700 cm^{-1} with increase in maturity (Fig. 3c, d). These bands are indicative of aromatic C–H out-of-plane deformations (Yen et al. 1984;

Ibarra et al. 1996) from different environments (Table 2). Note however that although the bands at 838 and 723 cm^{-1} are respectively commonly assigned to cyclic methylene (–CH$_2$–) and C$_{5+}$ methylene units (Guiliano et al. 1990), the fact that the intensities of the bands increase with increasing maturity (Fig. 3d) suggest they are more likely to be due to aromatic C–H deformation in agreement with Ibarra et al. (1996). The differences in the slopes of the plots in Fig. 3d suggest that the different aromatic C–H evolve at different rates during maturation.

The carbonyl (C=O) functionalities from ester (1768 cm^{-1}) and carboxyl group (1698 cm^{-1}) (Guiliano et al. 1990; Ibarra et al. 1996) decrease with increasing maturity while the highly conjugated carbonyl group of the quinone-type (1654 cm^{-1}) increases with maturity (Fig. 3e) in agreement with observations of Rouxhet et al. (1980) in coals. Lost of the ester and carboxyl groups

Fig. 3 The normalised areas of the absorption bands between 3000 and 700 cm^{-1}, obtained from curve-fitting of the FTIR spectra of the asphaltenes, plotted against vitrinite reflectance showing evolution of the different chemical functionalities with increasing maturity
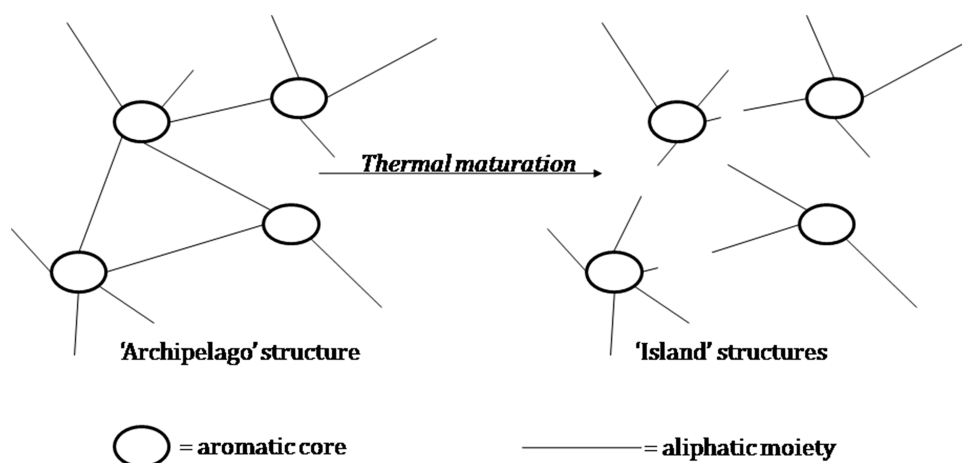

appear to precede loss of hydroxyl groups even in coals (Rouxhet et al. 1980). This indicates both the quinone-type carbonyl group and hydroxyl group are thermally more stable than ester and carboxyl groups in asphaltenes.

Although the bands at 1607 and 1497 cm^{-1} are commonly assigned to aromatic C=C stretching vibrations (Guiliano et al. 1990; Ibarra et al. 1996), in this study both bands decrease with increasing maturity (Fig. 3f) and correlate positively with O/C ratio ($R^2 > 0.80$; $p < 0.05$)

and thus might be due to oxygen functional groups possibly carboxylate ion (Nakanishi 1962).

Intensities of the six bands obtained from curve-fitting the spectral region between 1300 and 1000 cm^{-1} decrease with increasing maturity (Fig. 3g, h). Although these bands are quite difficult to assign due to the many functional groups that absorb in the region (Socrates 1980; Painter et al. 1981), the stiffness with which they decrease with increasing maturity suggests they might be due to various

428

Chin. J. Geochem. (2015) 34(3):422–430

Fig. 4 Simplified diagram illustrating thermal evolution of archipelago-type asphaltene molecules into island-type molecules with increasing thermal maturation

C–O functional groups from different environments (Table 2).

3.4 Possible implication to the molecular model of asphaltenes

The molecular structure of asphaltenes has been subject of intense investigations (Badre et al. 2006; Sabbah et al. 2010, 2011; Mullins et al. 2012; Alvarez-Ramírez and Ruiz-Morales 2013). Consequently, it has now been shown that the *dominant* molecular architecture is the Yen–Mullins model, which consider asphaltenes to have the so-called island structure consisting of a condensed heteroaromatic core with alkyl side chains (Mullins et al. 2012).

The observed structural evolution of asphaltenes with increase in thermal maturation may have a fundamental implication in asphaltene chemistry. First, asphaltene molecules from relatively immature sedimentary organic matter may be dominated by aliphatic moieties relative to aromatic moieties. Second, even if thermally immature asphaltene contain relatively significant archipelago-type molecular architecture, at higher degree of thermal maturity most of the inter-aromatic aliphatic linkages, as well as aliphatic side chains (Buch et al. 2003), would be lost to thermal dealkylation. This will ultimately generate complex, albeit more aromatic, molecular units dominated by island molecular architecture (the Yen–Mullins model) as illustrated in Fig. 4 in agreement with the observed dominant molecular architecture of asphaltenes from petroleum and artificially matured coal (Badre et al. 2006; Sabbah et al. 2011; Wu et al. 2013). It worth noting that thermal liquefaction of coal could result in its artificial thermal maturation and this could partly be the reason why coal asphaltenes have been reported to have higher relative carbon content and lower hydrogen content (and thus lower H/C atomic ratio) than the petroleum asphaltenes (Andrews et al. 2011). This therefore buttresses the need to investigate thermally immature asphaltenes (e.g. extracted from virgin immature coal) and particularly to determine the relative significance of the archipelago structures in them.

4 Conclusion

Thermal maturity was observed to affect the composition of asphaltenes from coals of different ranks. With increasing thermal stress, asphaltenes were observed to evolve towards an equilibrium structure or composition in which aromatic moieties become dominant over aliphatic moieties as a result of increasing aromatisation and dealkylation. Distribution of alkyl moieties shifts towards increasing proportions of the lower molecular weight homologues with increasing thermal maturity. The thermal stress also results in loss of oxygen functionalities from ester and carboxyl groups while hydroxyl groups appear to be more stable. The results are in agreement with the ultimate dominance of the island structure (the Yen–Mullins model) in petroleum asphaltenes.

References

Alboudwarej H, Beck J, Svrcek WY, Yarranton HW, Akbarzadeh K (2002) Sensitivity of asphaltene properties to separation techniques. Energy Fuels 16(2):462–469

Alvarez-Ramírez F, Ruiz-Morales Y (2013) Island versus archipelago architecture for asphaltenes: polycyclic aromatic hydrocarbon dimer theoretical studies. Energy Fuels 27(4):1791–1808

Chin. J. Geochem. (2015) 34(3):422–430

429

Andrews AB, Edwards JC, Pomerantz AE, Mullins OC, Nordlund D, Noringa K (2011) Comparison of coal-derived and petroleum asphaltenes by ^{13}C nuclear magnetic resonance, DEPT, and XRS. Energy Fuels 25(7):3068–3076

Badre S, Goncalvesa CC, Noringab K, Gustavsona G, Mullins OC (2006) Molecular size and weight of asphaltene and asphaltene solubility fractions from coals, crude oils and bitumen. Fuel 85:1–11

Baxby M, Patience RL, Bartle KD (1994) The origin and diagenesis of sedimentary organic nitrogen. J Pet Geol 17(2):211–230

Behar F, Pelet R, Roucache J (1984) Geochemistry of asphaltenes. Org Geochem 6:587–595

Buch L, Groenzin H, Buenorostro-Gonzalez E, Andersen SI, Lira-Galeana C, Mullins C (2003) Effect of hydrotreatment on asphaltene fractions. Fuel 82:1075–1084

Bunger JW, Li NC (eds) (1981) Chemistry of Asphaltenes, Advances in chemistry series 195, American Chemical Society, Washington D.C, p 260

Calemma V, Iwanski P, Nali M, Scotti R, Montanari L (1995) Structural characterization of asphaltenes of different origins. Energy Fuels 9(2):225–230

del Rio JC, Martin F, Gonzalez-Vila FJ, Verdejo T (1995) Chemical structural investigation of asphaltenes and kerogens by pyrolysis-methylation. Org Geochem 23(11–12):1009–1022

Dutta Majumdar R, Gerken M, Mikula R, Hazendonk P (2013) Validation of the Yen-Mullins model of athabasca oil-sands asphaltenes using solution-state 1H NMR relaxation and 2D HSQC spectroscopy. Energy Fuels 27(11):6528–6537

Galoppini M (1994) Asphaltene deposition monitoring and removal treatments: an experience in ultra deep wells. In: SPE Paper 27622 p 10

Groenzin H, Mullins OC (1999) Asphaltene molecular size and structure. J Phys Chem A 103(50):11237–11245

Guiliano M, Mille G, Doumenq P, Kister J, Muller JF (1990) Study of various rank french demineralized coals and maceral concentrates: band assignment of FTIR spectra afetr resolution enhancement using fourier deconvolution. In: Charcosset H (ed) advanced methodologies in coal characterisation (coal science and technology). Elsevier, Amsterdam, pp 399–417

Hammami A, Chang-Yen D, Nighswander JA, Stange E (1995) An experimental study of the effect of paraffinic solvents on the onset and bulk precipitation of asphaltenes. Fuel Sci Technol Int 13(9):1167–1184

Ibarra JV, Muñoz E, Moliner R (1996) FTIR study of the evolution of coal structure during the coalification process. Org Geochem 24(6–7):725–735

Khadim M, Sarbar M (1999) Role of asphaltene and resin in oil field emulsion. J Pet Sci Eng 23:213–221

Kokal SL, Sayegh SG (1995) Asphaltenes: the cholesterol of petroleum. In: SPE paper 29787. pp 169–81

Ma A, Zhang S, Zhang D (2008) Ruthenium-ion-catalyzed oxidation of asphaltenes of heavy oils in Lunnan and Tahe oilfields in Tarim Basin, NW China. Org Geochem 39(11):1502–1511

Maddams WF (1980) The scope and limitations of curve fitting. Appl Spectrosc 34:245–267

Mojelsky TW, Ignasiak TM, Frakman Z, McIntyre DD, Lown EM, Montgomery DS, Strausz OP (1992) Structural features of Alberta oil sand bitumen and heavy oil asphaltenes. Energy Fuels 6(1):83–96

Muhammad AB, Abbott GD (2013) The thermal evolution of asphaltene-bound biomarkers from coals of different rank: a potential information resource during coal biodegradation. Int J Coal Geol 107:90–95

Mullins OC (2009) Rebuttal to Strausz et al. regarding time-resolved fluorescence depolarization of asphaltenes. Energy Fuels 23:2845–2854

Mullins OC, Sabbah H, Eyssautier J, Pomerantz AE, Barré L, Andrews AB, Ruiz-Morales Y, Mostowfi F, McFarlane R, Goual L, Lepkowicz R, Cooper T, Orbulescu J, Leblanc RM, Edwards J, Zare RN (2012) Advances in asphaltene science and the yen-mullins model. Energy Fuels 26(7):3986–4003

Nakanishi K (1962) Infrared absorption spectroscopy. Nankodo Co Ltd, Tokyo, p 233

Painter PC, Snyder RW, Starsinic M, Coleman MM, Kuehn DW, Davis A (1981) Concerning the application of FT-IR to the study of coal: a critical assessment of band assignments and the application of spectral analysis programs. Appl Spectrosc 35:475–485

Peng P, Morales-Izquierdo A, Hogg A, Strausz OP (1997) Molecular structure of athabasca asphaltene: sulfide, Ether, and Ester Linkages. Energy Fuels 11(6):1171–1187

Peng P, Fu J, Sheng G, Morales-Izquierdo A, Lown EM, Strausz OP (1999) Ruthenium-ions-catalyzed oxidation of an immature asphaltene: structural features and biomarker distribution. Energy Fuels 13(2):266–277

Peters KE (1986) Guidelines for evaluating petroleum source rock using programmed pyrolysis. AAPG Bull 70:318–329

Rouxhet PG, Robin PL, Nicaise G (1980) Characterization of kerogens and their evolution by infrared spectroscopy. In: Durand B (ed) Kerogen: Insoluble organic matter from sedimentary rocks. Technip, Paris, pp 163–190

Sabbah H, Morrow AL, Pomerantz AE, Mullins OC, Tan X, Gray MR, Azyat K, Tykwinski RR, Zare RN (2010) Comparing laser desorption/laser ionization mass spectra of asphaltenes and model compounds. Energy Fuels 24(6):3589–3594

Sabbah H, Morrow AL, Pomerantz AE, Zare RN (2011) Evidence for island structures as the dominant architecture of asphaltenes. Energy Fuels 25(4):1597–1604

Shedid SA, Zekri AY (2006) Formation damage caused by simultaneous sulfur and asphaltene deposition. In: SPE paper 86553. pp 58–64

Sheu EY (2002) Petroleum asphaltene-propertiesm, characterization, and issues. Energy Fuels 16(1):74–82

Sheu EY, Mullins OC (eds) (1995) Asphaltenes: fundamentals and applications. Plenum Press, New York, p 245

Socrates G (1980) Infrared characteristic group frequencies: tables and charts, 2nd edn. Wiley, Chichester, p 249

Solli H, Leplat P (1986) Pyrolysis-gas chromatography of asphaltenes and kerogens from source rocks and coals–a comparative structural study. Org Geochem 10(1–3):313–329

Speight JG (2004) Petroleum asphaltenes—Part 1: asphaltenes, resins and the structure of petroleum. Oil Gas Sci Technol 59(5):467–477

Strausz OP, Mojelsky TW, Lown EM, Kowalewski I, Behar F (1999) Structural features of boscan and duri asphaltenes. Energy Fuels 13(2):228–247

Strausz OP, Safarik I, Lown EM, Morales-Izquierdo A (2008) A critique of asphaltene fluorescence decay and depolarization-based claims about molecular weight and molecular architecture. Energy Fuels 22(2):1156–1166

Trifilieff S, Sieskind O, Albrecht P (1992) Biological markers in petroleum asphaltenes: possible mode of incorporation. In: Moldowan JM, Albrecht P, Philp RP (eds) Biological markers in sediments and petroleum. Prentice Hall, New Jersey, pp 350–369

Weinberg VA, Yen TF, Murphy PDB, Gerstein BC (1983) Hypothetical average structures of two coal liquid asphaltenes from solid state 13 C nuclear magnetic resonance and 1 H nuclear magnetic resonance data. Carbon 21(2):149–156

William S (1985) Coal asphaltenes: a review. Fuel Process Technol 10(3):209–238

Wilson MA, Vassallo AM (1985) Developments in high-resolution solid-state13C NMR spectroscopy of coals. Org Geochem 8(5):299–312

Wilson MA, Pugmire RJ, Karas J, Alemany LB, Woolfenden WR, Grant DM, Given PH (1984) Carbon distribution in coal and coal macerals by cross-polarization magic angle spinning carbon-13 nuclear magnetic resonance spectroscopy. Anal Chem 56(933):43

Wu Q, Pomerantz AE, Mullins OC, Zare RN (2013) Laser-based mass spectrometric determination of aggregation numbers for petroleum- and coal-derived asphaltenes. Energy Fuels 28(1):475–482

Yen TF (1974) Structure of petroleum asphaltene and its significance. Energy Sources 1:447–463

Yen TF, Wu WH, Chilingar GV (1984) A study of the structure of petroleum asphaltenes and related substances by infrared spectroscopy. Energy Sources Part A 7(3):203–235